Hindawi
International Journal of Chemical Engineering
Volume 2022, Article ID 2292814, 14 pages
https://doi.org/10.1155/2022/2292814

Research Article

Kinetic Analysis of Aluminum Extraction from Ethiopian Kaolinite Using Hydrochloric Acid

Adamu Esubalew Kassa,[1] **Nurelegne Tefera Shibeshi**,[2] **and Belachew Zegale Tizazu**[1]

[1]*Department of Chemical Engineering, Addis Ababa Science and Technology University, Addis Ababa, Ethiopia*
[2]*School of Chemical and Bio-Engineering, Addis Ababa University, Addis Ababa, Ethiopia*

Correspondence should be addressed to Nurelegne Tefera Shibeshi; nurelegne.tefera@aait.edu.et

Received 22 March 2022; Revised 12 April 2022; Accepted 15 April 2022; Published 9 May 2022

Academic Editor: Nour Sh. El-Gendy

The aim of this study was kinetic investigations of aluminum extraction from Ethiopian kaolinite with hydrochloric acid. The effects of extraction parameters, namely, solid-to-liquid ratio (0.05, 0.075, 0.100, and 0.125 g·mL^{-1}), acid concentrations (2, 3, 4, and 5 M), reaction temperature (50, 60, 70, and 80°C), and time (20, 40, 60, 80, 100, 120, 140, 160, and 180 min), on yield of aluminum were investigated. The results revealed that the extraction yield of aluminum increased with increase of acid concentration, reaction temperature, and time and declined with increase of solid-to-liquid ratio. The kinetic analysis of aluminum extraction was evaluated using pseudohomogeneous, nucleation growth (Avrami), and shrinking core models. The results showed that kinetics of aluminum extraction were controlled by surface chemical reaction. The experimental results were well fitted by the shrinking core model of surface chemical reaction with first-order rate. The activation energy and the preexponential factor were 25.40 kJ·mol^{-1} and 0.949 cm·min^{-1}, respectively. The leached solution samples were crystallized using evaporation and concentrated hydrochloric acid pouring. The volume ratios of concentrated hydrochloric acid to the samples were from 0.30 to 0.90 (v/v). The crystallization efficiency of aluminum chloride hexahydrate crystals increased with volume of hydrochloric acid and crystallization time. The crystallization yield of aluminum chloride hexahydrate crystals reached 90%. This study's results clearly revealed that Ethiopian kaolinite could be a promising raw material to produce aluminum chloride hexahydrate, which could be used for water treatment application.

1. Introduction

Due to increase of aluminum demand in the global market and limited availability of bauxite in most countries, several studies have been conducted to produce aluminum from nonbauxite ores such as high-silica bauxite [1], boehmite-kaolinite bauxite [2], coal fly ash [3], coal gangue [4], red mud [5], coal mining waste [6], aluminum dross [7], and kaolinite [8–11]. The extraction of aluminum from high-silica bauxite, boehmite-kaolinite bauxite, coal fly ash, coal gangue, coal mining waste, and dross from waste in foundry industries may introduce impurities in the final product of aluminum, since these materials have high iron content. The availability of the raw materials is also limited in most countries. To overcome the problem of impurities and availability of the raw materials, kaolinite could be used as suitable and alternative raw material for aluminum extraction in various applications [8, 9, 12].

Kaolinite mineral is mainly made up of tetrahedral silicon oxide (SiO_4) and octahedral aluminum oxide (AlO_6) sheets, which form elemental clusters [13]. The mineral structure is built up among the elemental clusters through the hydrogen bond provided by hydroxyl ions of the octahedral sheets [14]. During kaolinite calcination, the hydroxyl structure could be removed and crystalline kaolinite could be changed to amorphous metakaolinite through dehydroxylation reaction [15–17]. The amorphous metakaolinite is highly reactive with mineral acids which indicate that kaolinite has to be calcined and transformed into metakaolinite for aluminum extraction [2, 8, 9, 12, 18].

The extraction of aluminum from calcined kaolinite has been carried out by mineral acids such as nitric acid,

hydrochloric acid, and sulfuric acid. The rate of aluminum extraction from metakaolinite using hydrochloric acid is the fastest over other mineral acids [8, 19–21]. Aluminum extraction using hydrochloric acid dissolution is advantageous over other acids' dissolution due to its selective precipitation and separation of aluminum chloride hexahydrate from leached solutions and removes silicon oxide at the first stage of the filtration process (silicon oxide is passive to react with hydrochloric acid), which simplifies the separation process and prevents the formation of harmful wastes [8, 10, 22]. The reaction between hydrochloric acid and metakaolinite is given in equation (1) and equation (2) [8, 21]. The aluminum extraction process is affected by calcination and extraction parameters such as calcination temperature, solid-to-liquid ratio, acid concentration, reaction temperature, and time [8, 10, 12, 23]. Furthermore, the extracted aluminum can be obtained in the form of aluminum chloride hexahydrate crystals, $AlCl_3{\cdot}6H_2O$ [9, 12]. The $AlCl_3{\cdot}6H_2O$ crystals can be obtained using direct crystallization [24], evaporation [6], direct crystallization [24], and pouring with concentrated hydrochloric acid [25]. The impurities present in the leached solution can be separated using crystallization [4, 6].

$$\frac{1}{6}Al_2O_3\,(s) + HCl\,(l) \longrightarrow \frac{1}{3}AlCl_3\,(l) + \frac{1}{2}H_2O\,(l), \quad (1)$$

$$Al_2Si_2O_7\,(s) + 6HCl\,(l) \longrightarrow 2AlCl_3\,(l) + 2SiO_2\,(s) + 3H_2O\,(l). \quad (2)$$

The reactions between solid and fluid are heterogeneous, which can be described by shrinking core, pseudohomogeneous, and Avrami models [23, 26, 27]. The shrinking core model assumes that the reaction rate may be controlled by a surface chemical reaction, diffusion through a fluid film, or diffusion through the product layer [28]. The pseudohomogeneous model is used for explaining the reaction process between flowing liquid and immobile solid [27]. The Avrami model is derived from systems in which the crystallization phenomenon occurs. The Avrami model may be used for explaining the rate equations in the noncatalytic solid-liquid reaction systems [29].

The kinetics of extraction of aluminum from several origins of kaolinite can be described using various models such as shrinking core, pseudohomogeneous, and nucleation growth models. The kinetics of extraction of aluminum from various origins of kaolinites such as Brazil, Turkey, Indonesia, USA, and China have been investigated; and extraction rates have been controlled by the first-order chemical reaction of unreacted core model [8, 9], the product layer diffusion [30], the product layer diffusion for one-stage extraction process and surface chemical reaction for two-stage extraction process [31], the second order chemical reaction [11], and chemical reaction of nucleation growth with Avrami model [23], respectively. The reasons for the difference in the kinetics model and rate controlling steps of aluminum extraction from various origins of kaolinite might be the variation of geographical location sources, calcination, and extraction process parameters. The mentioned literature results have shown the kinetics of aluminum extraction from various origins of kaolinite and the effect of process parameters on yield of aluminum to be investigated for different industrial applications.

In Ethiopia, kaolinite is one of the most available local minerals, and it can be used as raw material for various industrial applications. For instance, numerous investigations have been conducted on Ethiopian kaolinite for various applications such as synthesis of zeolite [32], adsorbent preparation [33], and ceramic membrane synthesis [34]. However, to the authors' knowledge, the kinetics of aluminum extraction from Ethiopian kaolinite using hydrochloric acid have not been investigated. This study is helpful in Ethiopia for production of aluminum chloride from locally available kaolinite, which could be used for water treatment application. Hence, this work aimed to investigate the kinetic analysis of aluminum extraction from Ethiopian kaolinite with hydrochloric acid, and the effects of extraction parameters, namely (the solid-to-liquid ratio, concentration of acid, reaction temperature, and time), were determined. The kinetic analysis of aluminum extraction was evaluated using pseudohomogeneous, nucleation growth (Avrami), and shrinking core models. The extracted aluminum content and the impurities present in the leached solution were determined using ultraviolent-visible spectrophotometer (UV-vis) and inductively coupled plasma-optical emission spectrometer (ICP-OES). Furthermore, the kaolinite, metakaolinite, residue after leaching, and extracted aluminum samples were characterized by X-ray fluorescence (XRF), X-ray diffractometer (XRD), Fourier transformer infrared spectrometer (FTIR), and scanning electron microscope (SEM).

2. Materials and Methods

2.1. Kaolinite Treatment and Extraction of Aluminum. The raw kaolinite was collected from Shakiso, Ethiopia. The raw kaolinite was soaked in ultrapure water to remove impurities and debris. The kaolinite was suspended with water. The suspension was separated from the insoluble solids residue. The suspension was left for settling under the action of gravity and separated from supernatant liquid. The wet kaolinite was dried overnight at 105°C. The dried samples were milled by mortar and pestle and then sieved by sieve analyzer (Elettronica Veneta S.p.A., CE IC-205/EV, Italy) to the particle size of 106 μm. They were then calcined using muffle furnace (MF 106, Turkey) at 700°C for 180 min to form metakaolinite for aluminum extraction experiments [35].

Hydrochloric acid (37% w/w) was used for the extraction of aluminum. The aluminum was extracted using hydrochloric acid solution at the designed extraction parameters. The extraction parameters were solid-to-liquid ratio (0.05, 0.075, 0.100, and 0.125 $g{\cdot}mL^{-1}$), acid concentrations (2, 3, 4, and 5 M), reaction temperature (50, 60, 70, and 80°C), and time (20, 40, 60, 80, 100, 120, 140, 160, and 180 min) at fixed stirring rate (1200 rpm). The leaching process was conducted using glass reactor (250 mL) with condenser and digital hotplate magnetic stirrer (MS-H280-Pro, DLAB Scientific Corporation Limited, China) with water bath at the designed

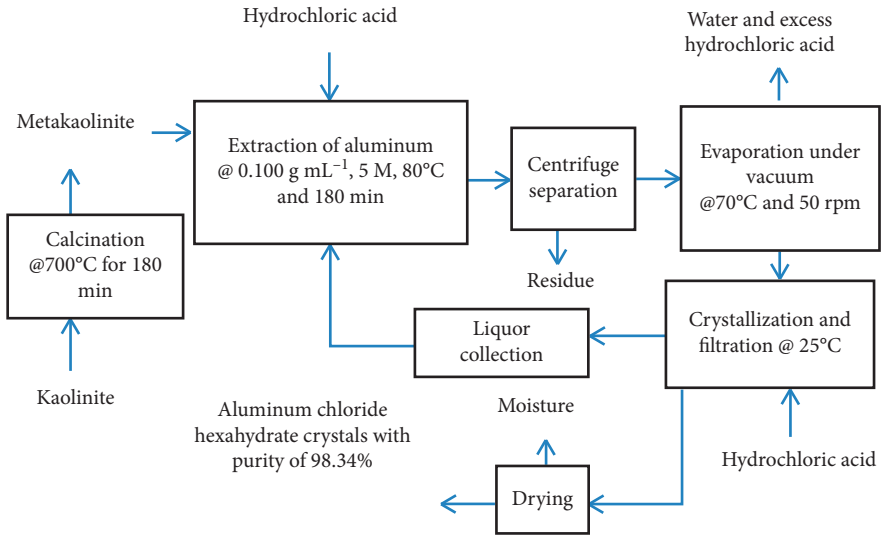

Figure 1: The process flow sheet of aluminum extraction from kaolinite.

extraction conditions. The volume of the acid was 150 mL in each experimental work and the mass of calcined kaolinite samples was varied from 7.50 to 18.75 g based on the experimental design. The extracted aluminum solutions in the slurry were separated using centrifuge (Funke Gerber Supervario-N 3680-2613, Germany) at 1200 rpm for 25 min. The extracted solution was evaporated and crystallized to separate the aluminum. The crystallized samples were dried in an oven and stored in plastic bags for further analysis. The process flow sheet of aluminum extraction from kaolinite is shown in Figure 1.

2.2. Determination of the Extracted Aluminum Content and Other Impurities. The content of aluminum in the extracted solutions was determined using ultraviolent-visible spectrometer (JASCO V-770, Japan). The standard aluminum solutions were prepared with some modification of the procedures described in literature [36–38]. The standard aluminum chloride hexahydrate (Blulux analytical reagent, 99%) was used to prepare standard solution and make calibration curve. The reagents of eriochrome cyanine red (ECR) dye ($C_{23}H_{15}Na_3O_9S$), hydrochloric acid, and sodium acetate solutions were prepared with concentrations of 0.2 mM, 0.2 M, and 0.2 mM, respectively. Then, 30 mL of aluminum chloride hexahydrate (ACH_s), 1.5 mL of ECR, 1 mL of hydrochloric acid, and 5 mL of sodium acetate were mixed together at room temperature, which could make aluminum-eriochrome cyanine red (Al-ECR) complex. The maximum absorbance wavelength of the aluminum-eriochrome cyanine red (Al-ECR) complex was determined by scanning it against the blank solution from 190 to 800 nm. Moreover, the calibration curve was prepared using standard solution concentrations of 2, 4, 6, 8, 10, 12, and 14 mg·L^{-1} of aluminum at fixed wavelength of 200 nm. The absorbance of extracted aluminum in the solution was measured at 200 nm, and the aluminum content in the solution was determined using the calibration curve. In addition, the compositions of other impurities contents in the leached solution were determined using inductively coupled plasma-optical emission spectrometer (OTPQ/1634 ULTIMA 2, HORIBA Scientific, France).

2.3. Kinetic Analysis of Aluminum Extraction. The kinetics of extraction of aluminum from calcined kaolinite were evaluated using various kinetics models such as pseudohomogeneous, nucleation growth, and shrinking core models. The kinetics of the pseudohomogeneous model are used for describing the reaction process between the flowing fluid and immobile solid. The rate equations for the pseudohomogeneous model are given in (3) and (4) [28].

Pseudohomogeneous first-order reaction is

$$-\ln(1 - X_B) = kt. \tag{3}$$

Pseudohomogeneous second-order reaction is

$$\frac{X_B}{(1 - X_B)} = kt, \tag{4}$$

where X_B is the conversion of solid; k is the rate constant of chemical reaction; and t is the reaction time.

The Avrami model may be used for explaining the rate equations in the noncatalytic solid-liquid reaction systems [29]. The logarithms form of the Avrami model is shown in the following equation:

$$\ln(-\ln(1 - X_B) = \ln k + n \ln t, \tag{5}$$

where X_B is the conversion of solid; k is the rate constant of chemical reaction; n is the nucleation model parameter; and t is the reaction time.

The shrinking core model assumes that the rate may be controlled by a surface chemical reaction, diffusion through a fluid film (external diffusion of extracted solute), or diffusion through the product layer (internal diffusion of acid concentration used for extraction agent). The rate equations

for the three limited cases are given in equations (6)–(12) [39]:

The fluid-solid reaction kinetics are of the following form:

$$A(l) + bB(s) \longrightarrow \text{product}(l). \quad (6)$$

Case 1. Chemical reaction controls the overall process:

$$1 - (1 - X_B)^{1/3} = k_c t, \quad (7)$$

where

$$k_c = \frac{bkC_A}{\rho_B r}. \quad (8)$$

Case 2. Diffusion through liquid film (stokes regime for small particles) controls:

$$1 - (1 - X_B)^{2/3} = k_f t, \quad (9)$$

where

$$k_f = \frac{2bD_eC_A}{\rho_B r^2}. \quad (10)$$

Case 3. Diffusion through the product layer control:

$$1 - 3(1 - X_B)^{2/3} + 2(1 - X_B) = k_d t, \quad (11)$$

where

$$k_d = \frac{6bD_eC_A}{\rho_B r^2}, \quad (12)$$

where X_B is conversion of solid particles B; k is the first-order rate constant for surface reaction; k_c is the rate constant of surface chemical reaction; k_f is the rate constant of diffusion through the liquid film; k_d is the rate constant of diffusion through the product layer; ρ_B is molar density of particle B; r is radius of particle; D_e is effective diffusion coefficient of liquid reactant in the product layer; C_A is bulk concentration of reactant liquid A; b is stoichiometric coefficient of solid particle B; and t is reaction time.

To determine the surface chemical reaction of the first-order rate constants (k values) at the reaction temperatures of 50, 60, 70, and 80°C, equation (8) was rearranged into equation (13). Further, the apparent activation energy and the preexponential factor of the kinetics of extraction of aluminum from calcined kaolinite were determined using Arrhenius relation as in equation (14) [28].

$$k = \frac{k_c \rho_B r}{bC_A}, \quad (13)$$

$$k = k_o \exp\left(-\frac{E_a}{RT}\right), \quad (14)$$

where b is the stoichiometry coefficient of A_2O_3, $b = 1/6$; C_A is the concentration of HCl, 5 M; ρ_B is the molar density of A_2O_3, $\rho_B = 9.35$ mole·L^{-1}; r is the radius of solid particles, $r = 0.0053$ cm; k_c is the rate constant of chemical reaction controlled (min^{-1}) at 50, 60, 70, and 80°C; k is the surface chemical reaction first-order rate constant (cm·min^{-1}); k_o is the preexponential factor (cm·min^{-1}); E_a is the activation energy (kJ mol^{-1}); T is absolute temperature (K); and R is the gas constant ($R = 8.314 \times 10^{-3}$ kJ·mol^{-1}·K^{-1})

2.4. Crystallization of Leached Solution. The crystallization of leached solutions was conducted using some modification of the method described in the literature [4, 6, 25]. The leached solutions were evaporated using vacuum rotary evaporator (ML-E14-2050, Maalab Scientific Equipment Private Limited, India) at 70°C and 50 rpm until the crystals of aluminum chloride hexahydrate were observed. The concentrated solutions with semicrystallized aluminum chloride hexahydrate were allowed to cool at room temperature and transferred into the crystallizer. To increase crystallization efficiency, concentrated hydrochloric acid (37%) was used. The volume ratios of concentrated hydrochloric acid to the samples were from 0.30 to 0.90 (v/v). The crystallization time was considered from 8 to 56 h. The crystals were decanted at the bottom of the crystallizer and the liquor was suspended over the crystal layer. The liquor was filtered, and the crystals were separated and dried in the oven with ceramic trays at 80°C for 6 h. The samples were stored in closed plastic bags for analysis.

2.5. Characterization of Kaolinite, Metakaolinite, Residue, and Extracted Aluminum. The samples' chemical compositions were determined using X-ray fluorescence (XRF) (BTX-528, USA). The samples were scanned by XRF at 1.54 nm wavelength of kαCu anode and X-ray tube voltage of 30 kV. The kaolinite, calcined kaolinite (metakaolinite), residue after leaching (hereafter called residue), and extracted aluminum samples' crystalline structures were characterized using X-ray diffraction (SHIMDZU XRD-7000, Japan) at cooling temperature of −45°C, 1.54 nm wavelength of kαCu anode, X-ray tube voltage of 40 kV, specimens step scan rate of 3 min^{-1}, and 2θ angles from 5 to 60°. The XRD reflection peaks were analyzed by XPowder software (version 2010). The functional group bands of the kaolinite, metakaolinite, residue, and extracted aluminum samples were characterized using Fourier transformer infrared spectrometer with attenuation total reflection and detector of DTGS KBr (iS50 ABX smart iTX, USA). The middle infrared reflection wavenumber absorption bands were from 4000 to 400 cm^{-1} with 32 numbers of scans and resolution of 16 cm^{-1}. Moreover, the morphologies of the samples were also analyzed using scanning electron microscope (JMC-6000Plus benchtop SEM, JEOL Ltd, Japan). The images of the samples were taken at 10 kV and 20 m.

3. Results and Discussion

3.1. Effect of Extraction Parameters on the Yield of Aluminum. Figures 2(a)–2(c) depict the effects of solid-to-liquid ratio, acid concentration, and reaction temperature on the yield of

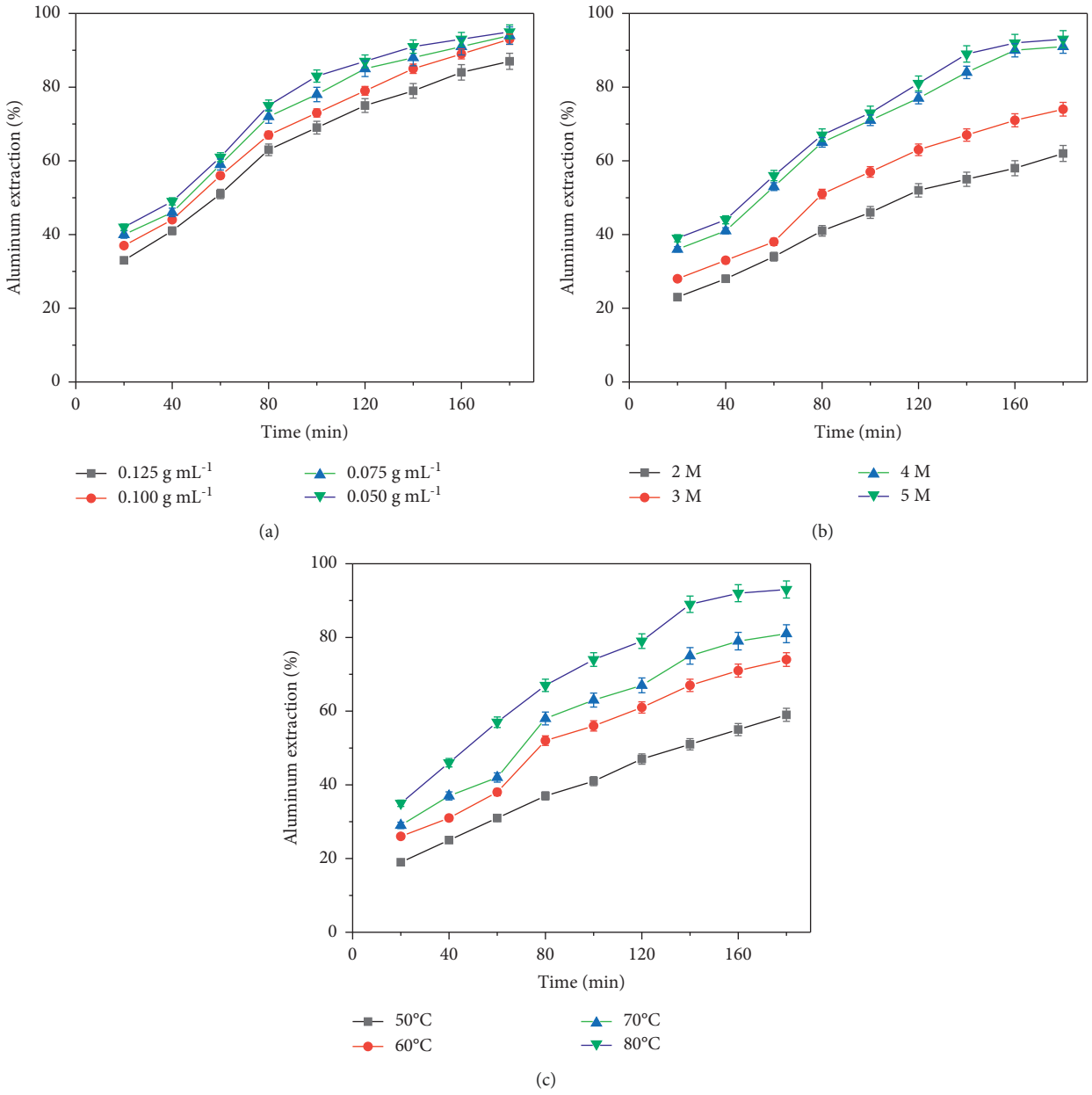

Figure 2: Effects of (a) solid-to-liquid ratio from 0.050 to 0.125 g·mL^{-1} at 5 M and 80°C, (b) acid concentration from 2 to 5 M at 0.100 g·mL^{-1} and 80°C, and (c) reaction temperature from 50 to 80°C at 0.100 g·mL^{-1} and 5 M on the extraction yield of aluminum.

aluminum, respectively. The fraction of extracted aluminum increased as the acid concentration and reaction temperature were increased, and the solid-to-liquid ratio was reduced. Figure 2(a) shows that the fraction of the extracted aluminum increased as the solid-to-liquid ratio was reduced. The fraction of the maximum extracted aluminum increased from 87 to 95% as the solid-to-liquid ratio was reduced from 0.125 to 0.005 g·ml^{-1} at 5 M, 80°C, and 180 min. Even though the yield of aluminum was highest at the lowest solid-to-liquid ratio, the recovery of the acid solution required more energy and time, which could increase the production cost. The yield of 93% was obtained at the solid-to-liquid ratio of 0.100 g·ml^{-1}, which could be the appropriate solid-to-liquid ratio to reduce excess acid recovery cost with maximum extraction yield of aluminum. Figure 2(b) reveals that the fraction of yield of aluminum was increased with the acid concentration. As the acid concentration was increased from 2 to 5 M, the fraction of the maximum extracted aluminum increased from 62 to 93% at 80°C, 0.100 g·mL^{-1}, and 180 min. Moreover, Figure 2(c) displays the effect of reaction temperature on the extraction yield of aluminum. The extraction yield of aluminum increased with the reaction temperature. The extraction yield of aluminum increased from 54 to 92% as the reaction temperature was increased from 50 to 80°C at 5 M, 0.100 g·mL^{-1}, and 180 min. The extraction yield of aluminum increased with increase of acid concentration and reaction temperature and decrease of solid-to-liquid ratio [8, 9, 23].

Table 1: The regression correlation coefficients and rate constants for aluminum extraction at various solid-to-liquid ratios from 0.050 to 0.125 g·mL^{-1}.

Model	Rate equation	The regression correlation coefficients and rate constants (k_i[1]) for extraction of aluminum at various solid-to-liquid ratios from 0.050 to 0.125 g·mL^{-1}							
		0.050		0.075		0.100		0.125	
		R^2	k_i	R^2	k_i	R^2	k_i	R^2	k_i
Shrinking core	$1-(1-X_B)^{1/3}=k_ct$	0.993	3.09×10^{-3}	0.994	2.94×10^{-3}	0.984	2.81×10^{-3}	0.983	2.36×10^{-3}
	$1-(1-X_B)^{2/3}=k_ft$	0.954	3.71×10^{-3}	0.969	3.65×10^{-3}	0.974	3.52×10^{-3}	0.982	3.28×10^{-3}
	$1-3(1-X_B)^{2/3}+2(1-X_B)=k_dt$	0.978	4.16×10^{-3}	0.976	4.03×10^{-3}	0.967	3.99×10^{-3}	0.965	3.50×10^{-3}
Pseudohomogeneous	$-\ln(1-X_B)=kt$	0.975	1.57×10^{-2}	0.971	1.46×10^{-2}	0.964	1.37×10^{-2}	0.955	1.12×10^{-2}
	$X_B/(1-X_B)=kt$	0.936	3.76×10^{-2}	0.901	5.87×10^{-2}	0.893	8.55×10^{-2}	0.873	1.09×10^{-1}
Avrami	$\ln(-\ln(1-X_B)=\ln k+n\ln t$	0.974	3.26×10^{-2}	0.962	3.37×10^{-2}	0.961	3.49×10^{-2}	0.960	3.58×10^{-2}
	Model parameter (n)	0.773		0.814		0.832		0.841	

[1]For surface chemical reaction controlled, $k_i=k_c$; for diffusion through liquid controlled, $k_i=k_f$; and, for diffusion though product layer controlled , $k_i=k_d$.

Table 2: The regression correlation coefficients and rate constants for extraction of aluminum at various acid concentrations from 2 to 5 M.

Model	Rate equation	The regression correlation coefficients and rate constants (k_i) for extraction of aluminum at various acid concentrations from 2 to 5 M							
		2 M		3 M		4 M		5 M	
		R^2	k_i	R^2	k_i	R^2	k_i	R^2	k_i
Shrinking core	$1-(1-X_B)^{1/3}=k_ct$	0.991	1.22×10^{-3}	0.993	1.72×10^{-3}	0.983	2.64×10^{-3}	0.992	2.87×10^{-3}
	$1-(1-X_B)^{2/3}=k_ft$	0.984	2.05×10^{-3}	0.983	2.64×10^{-3}	0.972	3.36×10^{-3}	0.974	3.61×10^{-3}
	$1-3(1-X_B)^{2/3}+2(1-X_B)=k_dt$	0.970	1.12×10^{-3}	0.971	1.81×10^{-3}	0.972	3.37×10^{-3}	0.974	3.58×10^{-3}
Pseudohomogeneous	$-\ln(1-X_B)=kt$	0.974	4.36×10^{-3}	0.972	6.24×10^{-3}	0.964	1.13×10^{-2}	0.963	1.33×10^{-2}
	$X_B/(1-X_B)=kt$	0.981	8.75×10^{-3}	0.973	1.60×10^{-2}	0.863	5.38×10^{-2}	0.824	6.92×10^{-2}
Avrami	$\ln(-\ln(1-X_B)=\ln k+n\ln t$	0.973	3.17×10^{-2}	0.952	3.27×10^{-2}	0.953	3.40×10^{-2}	0.950	3.44×10^{-2}
	Model parameter (n)	0.623		0.704		0.803		0.812	

[2]LOI: loss on ignition from TGA analysis.

3.2. Kinetics Analysis of Aluminum Extraction from Kaolinite

3.2.1. Kinetics Analysis of Aluminum Extraction at Various Solid-to-Liquid Ratios. Table 1 describes the regression correlation coefficients and rate constants of the kinetics of the extraction of aluminum at various solid-to-liquid ratios from 0.050 to 0.125 g·mL^{-1}. The regression coefficients of the shrinking core model of chemical reaction with first-order kinetics were the largest compared to the others. The regression coefficients (R^2) were from 0.983 to 0.994 for the first-order chemical reaction kinetics of shrinking core model. The results confirmed that the rate of extraction of aluminum was controlled by surface chemical reaction. The kinetics were well described by the first-order chemical reaction shrinking core model.

3.2.2. Kinetics Analysis of Aluminum Extraction at Various Acid Concentrations. The regression correlation coefficients and rate constants of the kinetics of aluminum extraction at acid concentrations from 2 to 5 M are shown in Table 2. The regression coefficients of the surface chemical reaction with first-order kinetics model were the largest compared to the others. The regression coefficients (R^2) were from 0.983 to 0.993 for the first-order chemical reaction kinetics of shrinking core model. The results revealed that the rate of extraction of aluminum was controlled by surface chemical reaction. The kinetics were well described by first shrinking core model of first-order reaction.

3.2.3. Kinetics Analysis of Extraction of Aluminum at Various Reaction Temperatures. Table 3 describes the regression correlation coefficients and rate constants of the kinetics of extraction of aluminum from 50 to 80°C. The regression coefficients of the surface chemical reaction with first-order kinetics model were the largest over the diffusion through product layer, diffusion through fluid film, pseudohomogeneous first-order and second-order reactions, and Avrami model kinetics regression coefficients. The regression coefficient (R^2) of the first-order chemical reaction kinetics of shrinking core model at various reaction temperatures was 0.993, which was close to unity. The results indicated that the rate of extraction of aluminum was controlled by surface chemical reaction. The kinetics were well described by surface chemical reaction with first-order rate. The apparent activation energy of the kinetics of extraction of aluminum from calcined kaolinite was determined using Arrhenius relation. The natural logarithm of the Arrhenius relation provides a linear equation.

3.2.4. Shrinking Core Model of Surface Chemical Reaction with First-Order Reaction Kinetics. Figures 3(a)–3(d) show the plots of shrinking core model of surface chemical reaction rate controlled step with first-order reaction rate at various solid-to-liquid ratio, acid concentrations, reaction temperatures, and the activation energy, respectively. Figure 3(a) depicts the regression plots of the surface

Table 3: The regression correlation coefficients and rate constants for extraction of aluminum at various reaction temperatures from 50 to 80°C.

Model	Rate equation	The regression correlation coefficients and rate constants (k_i) at various reaction temperatures from 50 to 80°C							
		50°C		60°C		70°C		80°C	
		R^2	k_i	R^2	k_i	R^2	k_i	R^2	k_i
Shrinking core	$1-(1-X_B)^{1/3}=k_c t$	0.991	1.23×10^{-3}	0.984	1.74×10^{-3}	0.993	2.02×10^{-3}	0.994	2.86×10^{-3}
	$1-(1-X_B)^{2/3}=k_f t$	0.971	1.77×10^{-3}	0.964	2.61×10^{-3}	0.972	2.95×10^{-3}	0.963	3.64×10^{-3}
	$1-3(1-X_B)^{2/3}+2(1-X_B)=k_d t$	0.972	9.86×10^{-4}	0.974	1.82×10^{-3}	0.971	2.27×10^{-3}	0.964	3.74×10^{-3}
Pseudohomogeneous	$-\ln(1-X_B)=kt$	0.963	4.27×10^{-3}	0.961	6.79×10^{-3}	0.954	7.94×10^{-3}	0.953	1.39×10^{-2}
	$X_B/(1-X_B)=kt$	0.973	7.47×10^{-3}	0.971	1.58×10^{-2}	0.943	2.30×10^{-2}	0.843	7.23×10^{-2}
Avrami	$\ln(-\ln(1-X_B)=\ln k+n\ln t$	0.972	2.90×10^{-2}	0.970	2.99×10^{-2}	0.963	3.21×10^{-2}	0.942	3.27×10^{-2}
	Model parameter (n)	0.634		0.723		0.742		0.820	

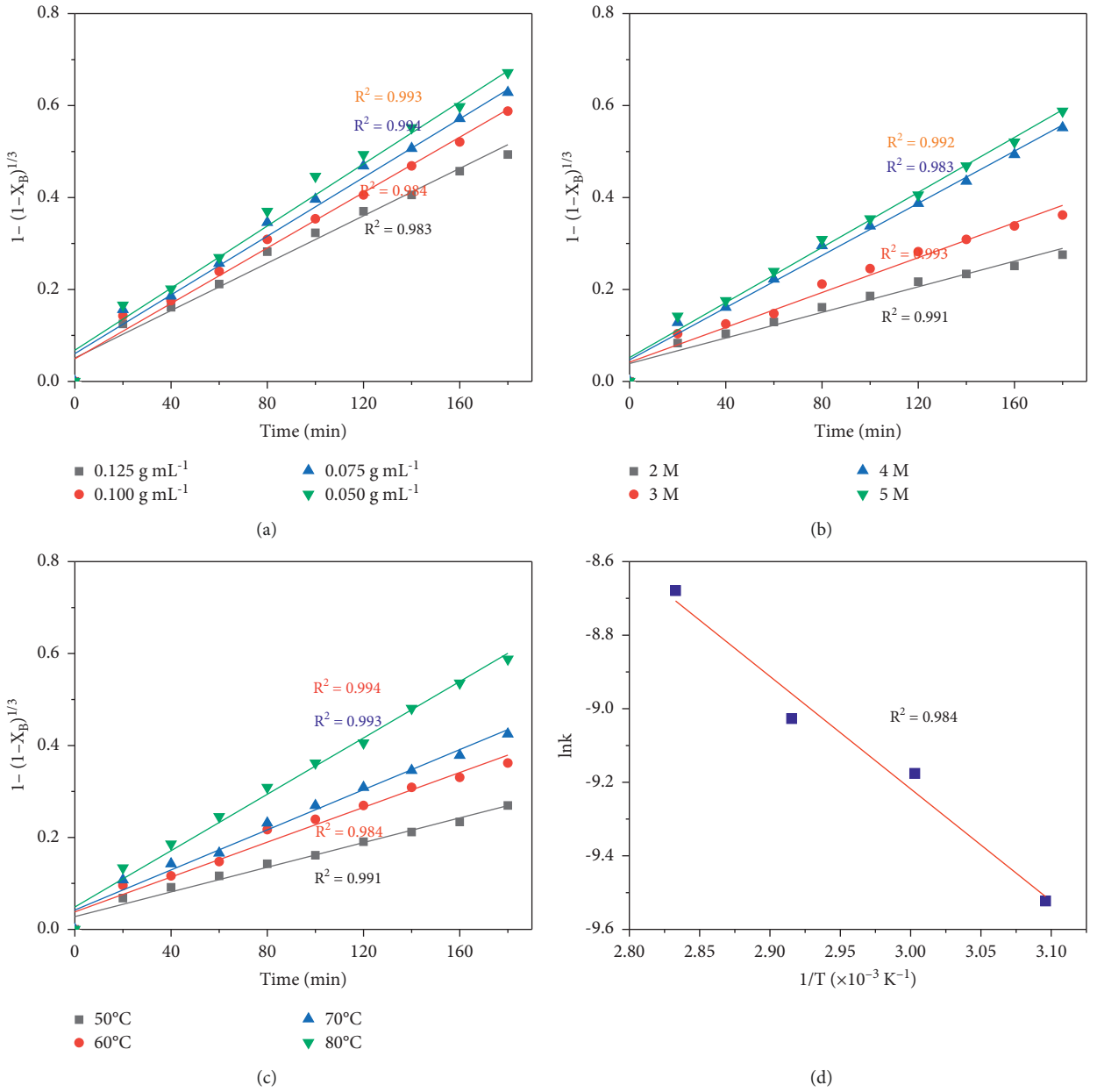

Figure 3: The regression plots of first-order reaction kinetics of shrinking core model at various (a) solid-to-liquid ratios from 0.05 to 0.125 g·mL^{-1}, (b) acid concentrations from 2 to 5 M, and (c) reaction temperatures from 50 to 80°C; (d) the Arrhenius plot of the first-order chemical reaction.

Table 4: The first-order reaction rate constant of surface chemical reaction at various reaction temperatures from 50 to 80°C.

Reaction temperature (°C)	50	60	70	80
First-order reaction rate constant (cm min^{-1})	7.32×10^{-5}	1.04×10^{-4}	1.20×10^{-4}	1.70×10^{-4}

chemical reaction with first-order rate for solid-to-liquid ratios from 0.050 to 0.125 g·mL^{-1}. As the solid-to-liquid ratio was increased, the reaction rate constant decreased. The rate constants were 3.09×10^{-3}, 2.94×10^{-3}, 2.81×10^{-3}, and 2.36×10^{-3} min^{-1} at 0.050, 0.075, 0.100, and 0.125 g·mL^{-1}, respectively. In the lowest solid-to-liquid ratio, the calcined kaolinite obtained enough acid solution for extraction of aluminum and the reaction rate was relatively the fastest. This result confirmed that the rate of the reaction was relatively the fastest at the lowest solid-to-liquid ratio.

For the extraction of aluminum at various acid concentrations from 2 to 5 M, the regression plots of the shrinking core model of the surface chemical reaction rate controlled step with the first-order reaction rate are depicted in Figure 3(b). The reaction rate constant was increased with acid concentration. The rate constants were 1.22×10^{-3}, 1.72×10^{-3}, 2.64×10^{-3}, and 2.87×10^{-3} min^{-1} at 2, 3, 4, and 5 M, respectively. The highest conversion was obtained at the highest acid concentration which revealed that the highest acid concentration reacted rapidly with metakaolinite and kaolinite for extraction of aluminum.

Figure 3(c) represents the regression plots of the shrinking core model of surface chemical reaction rate controlled step of the first-order reaction rate at various temperatures for extraction of aluminum. The rate constants (k_c values, Table 3) were 1.23×10^{-3}, 1.74×10^{-3}, 2.01×10^{-3}, and 2.86×10^{-3} min^{-1} at 50, 60, 70, and 80°C, respectively. Thus, the surface chemical reactions of the first-order reaction rate constants (k values from equation (13)) were 7.32×10^{-5}, 1.04×10^{-4}, 1.20×10^{-4}, and 1.70×10^{-4} cm·min^{-1} at 50, 60, 70, and 80°C, respectively, as depicted in Table 4.

Figure 3(d) illustrates the plots of the natural logarithm of the rate constants, ln (k), versus the inverse of the reaction temperature, $1/T$. The ln (k) versus $1/T$ values were plotted, and a straight line was obtained. The apparent activation energy was determined from the slope of the straight line of ln (k) versus $1/T$ plot. The linearized Arrhenius relation regression correlation coefficient (R^2) was 0.98, which confirmed that the dependency of the shrinking core model kinetics first-order reaction rate constant on reaction temperature was governed by the Arrhenius relation. The apparent activation energy and the preexponential factor of the kinetics of extraction of aluminum from calcined kaolinite were 25.40 kJ·mol^{-1} and 0.949 cm·min^{-1}, respectively. Thus, the kinetics of extraction of aluminum final rate equation are written in equation (15). The reactions with high activation energies are very sensitive for temperature; and reactions with low activation energies are relatively less sensitive for temperature [28]. In this work, the activation energy was relatively lower, which revealed that the reaction of calcined kaolinite and hydrochloric acid was less sensitive for reaction temperature. Moreover, Figure 4 demonstrates the kinetics model of aluminum extraction from kaolinite controlled by surface chemical reaction and photos of kaolinite and extracted aluminum chloride hexahydrate.

$$1 - \left(1 - X_B\right)^{1/3} = 3.19 C_A \exp\left(\frac{-25.4}{RT}\right) t, \tag{15}$$

where X_B is conversion of A_2O_3; C_A is concentration of HCl (M); t is reaction time (min); T is absolute temperature (K); and R is the gas constant ($R = 8.314 \times 10^{-3}$ kJ·mol^{-1}·K^{-1}).

3.3. Characteristics of the Kaolinite, Metakaolinite, and Residue

3.3.1. Chemical Compositions. The main chemical compositions of Ethiopian kaolinite were silicon oxide (55.76%), aluminum oxide (32.02%), and loss of ignition (11.17%) [35]. Table 5 depicts the chemical compositions of metakaolinite and residue after acid leaching. The main chemical compositions of Ethiopian metakaolinite were silicon oxide (62.84%) and aluminum oxide (36.09%) as illustrated in (a) in Table 5. Furthermore, chemical composition of the residue from acid leaching was mainly silicon oxide (85.54%) as shown in (b) in Table 5. The results of this study showed that the Ethiopian kaolinite could be the potential source for aluminum extraction.

3.3.2. XRD, FTIR, and SEM Analysis of Kaolinite, Metakaolinite, and Residue. The XRD peaks of kaolinite, calcined kaolinite (metakaolinite), and residue after leaching are shown in Figure 5. The XRD peaks of kaolinite are depicted in Figure 5(a). The high intensity peaks of kaolinite were detected as 9.13, 12.0, 18.14, 20.6, 24.6, 28.2, 35.7, 38.7, 45.6, and 55.1 with the Miller indices of (004), (001), (004), (200), (1 1 0), (021), (1 3 1), (003), (123), and (240), respectively, at the 2θ angles. The crystal structure of kaolinite was monoclinic, which has the unit cell axes of $a = 5.14$ Å, $b = 8.92$ Å, and $c = 14.53$ Å with the angles of $\alpha = 90°$, $\beta = 100.2°$, and $\gamma = 90°$. The quartz high intensity peaks were also observed at the 2θ angles of 21.1 and 26.7 with Miller indices of (100) and (101), respectively. Figure 5(b) shows the XRD peaks of metakaolinite, which was formed at 700°C. The XRD reflections of metakaolinite had amorphous structure with the presence of the quartz peaks. The crystalline peaks of kaolinite vanished during calcination, which revealed that crystalline kaolinite was transformed into amorphous metakaolinite via dehydroxylation reaction. Figure 5(c) displays the XRD results of the residue after leaching. The quartz peaks were detected in the residue XRD results which confirmed that silicon oxide was not dissolved with hydrochloric acid during leaching. The results were in agreement with previous results [14, 15].

Figure 6 describes the FTIR curves of kaolinite and calcined kaolinite. Figure 6(a) illustrates the FTIR curve of

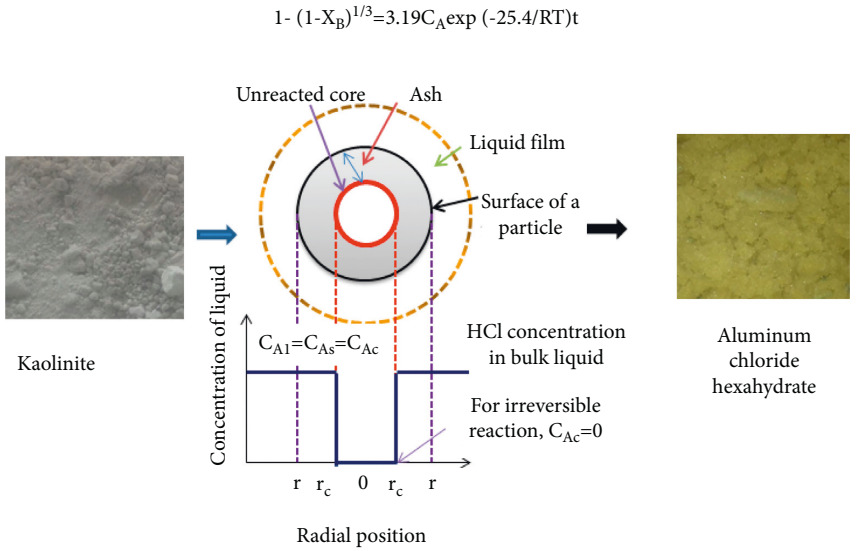

Figure 4: The kinetic model of aluminum extraction from kaolinite controlled by surface chemical reaction and the photos of kaolinite and extracted aluminum chloride hexahydrate crystals from leaching at 0.10 g·mL^{-1}, 5 M, 80°C, and 180 min.

Table 5: Chemical compositions of Ethiopian metakaolinite at 700°C for 180 min and residue.

	Oxides	SiO_2	Al_2O_3	TiO_2	K_2O	Na_2O	MgO	Fe_2O_3	LOI[2]
(a) Metakaolinite	Composition (%)	62.84	36.09	0.38	0.27	0.18	0.19	0.04	0.01
(b) Residue	Composition (%)	85.54	3.44	0.52	0.02	0.01	0.02	0.01	10.43

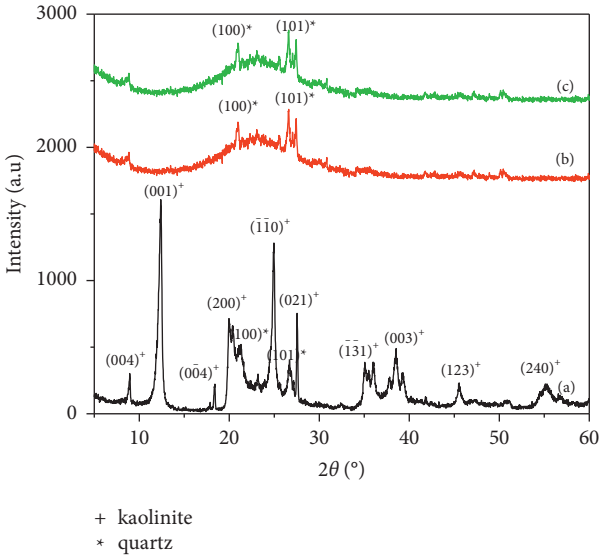

Figure 5: XRD peaks of (a) kaolinite, (b) metakaolinite at 700°C for 180 min, and (c) residue after leaching at 0.10 g·mL^{-1}, 5 M, 80°C, and 180 min.

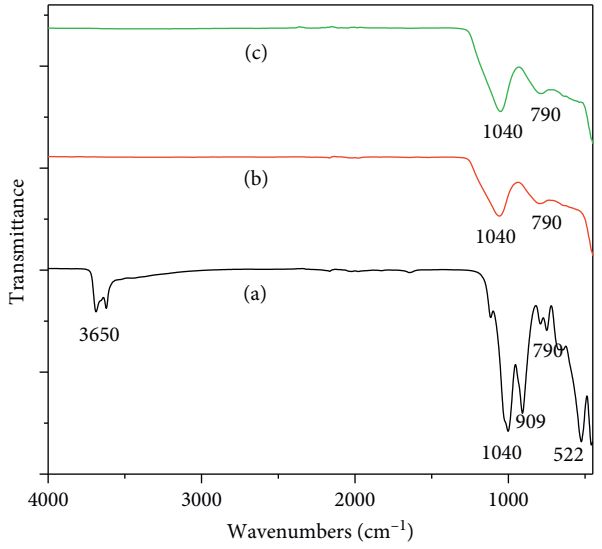

Figure 6: FTIR curves of (a) kaolinite, (b) metakaolinite at 700°C for 180 min, and (c) residue after leaching at 0.10 g·mL^{-1}, 5 M, 80°C, and 180 min.

kaolinite. The characteristic band was detected at 3650 due to stretching of hydroxides of water molecules in kaolinite. The band at 1040 cm^{-1} was due to the stretching vibrations of Si-O-Si, and the band at 790 cm^{-1} was the characteristic of quartz which was attributed to O-Si-O bending vibrations. The Al-OH group transitional vibration was detected at 909 cm^{-1}, and the bending of Si-O-Al^{VI} octahedral coordinating vibration band was obtained at 522 cm^{-1}. Figure 6(b) shows the FTIR curve of calcined kaolinite at 700°C. The hydroxide bands disappeared at the calcination temperature of 700°C which confirmed that kaolinite was transformed into metakaolinite. Furthermore, the Al-OH group transitional vibration at 908 cm^{-1} and the bending of Si-O-Al^{VI} octahedral coordinating vibration at 522 cm^{-1} also

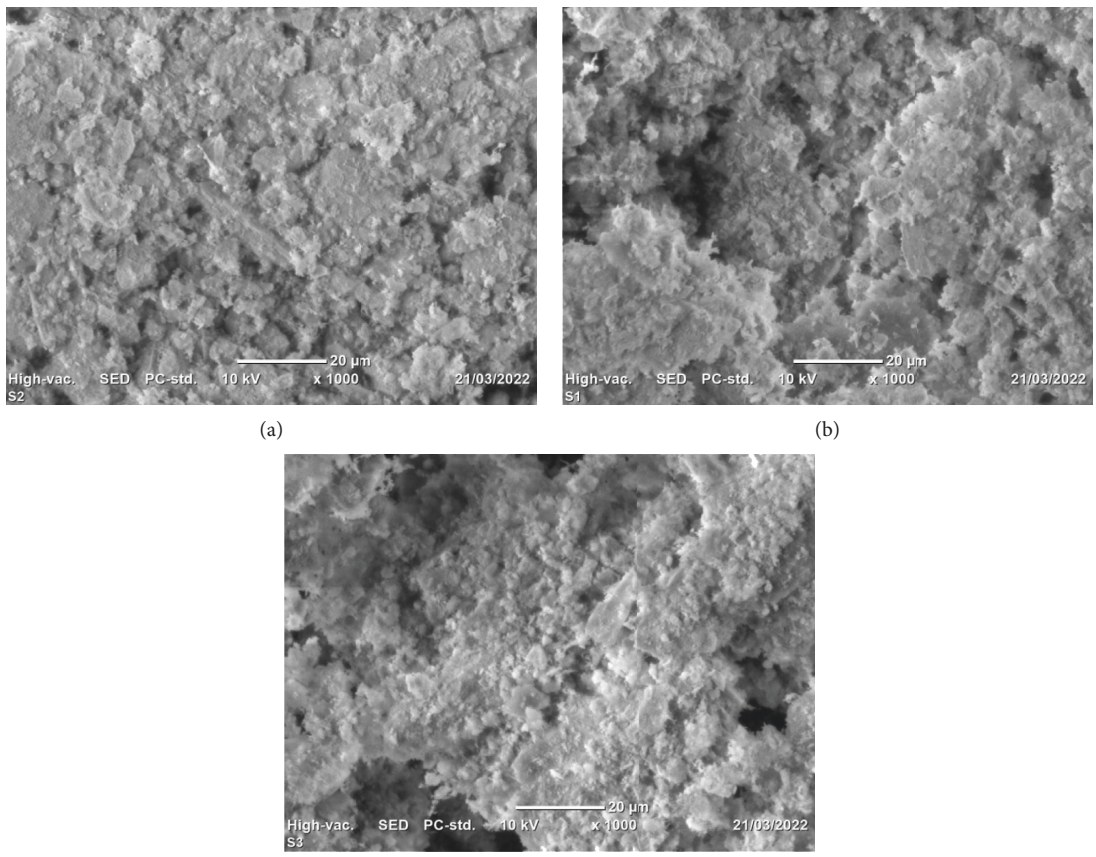

(a) (b)

(c)

Figure 7: SEM results at 10 kV and 20 μm for (a) kaolinite, (b) metakaolinite, and (c) residue after leaching at 0.10 g·mL^{-1}, 5 M, 80°C, and 180 min.

vanished. However, the bands at 1040 and 790 cm^{-1} were observed, which were attributed to O-Si-O bending vibrations due to survival of quartz at 700°C. Figure 6(c) illustrates the FTIR curve of residue after leaching. The bands at 1040 and 790 cm^{-1} were observed, which were attributed to O-Si-O bending vibrations due to survival of quartz during leaching process. These results were in agreement with previous literature [16, 17].

Figure 7 shows the morphology of (a) kaolinite, (b) calcined kaolinite, and (c) residue at 10 kV and 20 μm. The SEM images' results indicated that kaolinite, calcined kaolinite, and the residue surface morphologies had heterogeneous sizes. Surface morphology change was observed for calcined kaolinite. This indicated that the calcination temperature could modify the surface morphology of the initial kaolinite. Moreover, the SEM result of the residue from leaching showed some change in shape and porosity due to acid leaching. This revealed that the residue was in the form of micro-porous silica [40].

3.4. Characteristics of the Extracted Aluminum

3.4.1. Chemical Compositions of the Leached Solution. The chemical composition of the leached solution is shown in (a) in Table 6. The leached solution was mainly aluminum chloride. In the leached solution, potassium, sodium, magnesium, and iron ions were detected as impurities. The compositions of impurities present in the leached solution were reduced and separated from final product via crystallization and filtration processes. (b) in Table 6 depicts the chemical composition of aluminum chloride hexahydrate crystals. The result revealed that the purity of aluminum chloride hexahydrate crystals was 98.34%. In the literature, aluminum chloride hexahydrate with purity of 96.8% has been obtained from coal gangue [4].

3.4.2. Crystallization Results. The effect of volume ratio of concentrated hydrochloric acid and time on crystallization and recovery of extracted aluminum chloride hexahydrate crystals at 25°C is shown in Figure 8. During crystallization of leached solution, selective crystallization of aluminum chloride hexahydrate crystals occurred and other impurities remained in the solution. The crystallization efficiency and recovery of aluminum chloride hexahydrate crystals increased with volume of hydrochloric acid and crystallization time. The crystallization yield of aluminum chloride hexahydrate crystals reached 90%. The results revealed that this study required less volume of hydrochloric acid with better crystallization efficiency of aluminum chloride hexahydrate crystals as compared with the literature [4, 6, 25].

Table 6: Chemical compositions of the leached solution and aluminum chloride hexahydrate crystals.

(a) Chemical compositions of the leached solution					
Component	A1	Na	K	Fe	Mg
Concentration ($g{\cdot}L^{-1}$)	25.4	0.14	0.24	0.02	0.15
(b) Chemical composition of aluminum chloride hexahydrate (ACH) crystals					
Component	$A1Cl_3{\cdot}6H_2O$	NaCl	KCl	$FeCl_3$	$MgCl_2$
Composition (%)	98.34	0.50	0.74	0.01	0.41

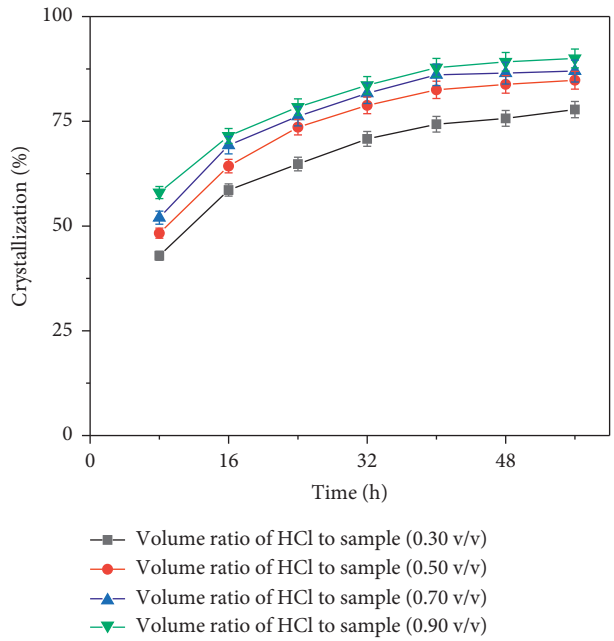

Figure 8: Effect of the volume ratio of concentrated hydrochloric acid to the samples from 0.30 to 0.90 (v/v) and time from 8 to 56 h on aluminum chloride hexahydrate crystallization at 25°C.

3.4.3. XRD, FTIR, and SEM Analysis of Extracted Aluminum. The XRD result of extracted aluminum is illustrated in Figure 9(a). The crystal structure of extracted aluminum was trigonal, which has the unit cell axes of $a = b = c = 7.85$ Å with the angles of $\alpha = \beta = \gamma = 97^{\circ}$. The crystal structure's Miller indices were (110), (012), (300), (321), (113), (122), (220), (232), (312), (042), (134), (120), and (004) at 2θ angles of 15.2, 17.3, 24.1, 26.3, 27.2, 27.8, 30.4, 35.1, 39.4, 41.5, 44.2, 52.1, and 54.5, respectively. The crystalline structure results revealed that the extracted aluminum was in the form of aluminum chloride hexahydrate [41].

The FTIR curves of the extracted aluminum functional groups bands are illustrated in Figure 9(b). The extracted aluminum functional groups bands were identical with the characteristics of aluminum chloride hexahydrate, which indicated that the extracted aluminum was in the form of aluminum chloride hexahydrate. The functional groups bands were detected at the wavenumbers of 3022, 2409, 1633, 826, and 523 cm^{-1} which were due to stretching vibration of -OH groups, bending vibration of -OH groups of water molecules, asymmetric stretching vibration of Al-O-Al, bending vibration of Al-OH-Al, and bending vibration of Al-OH in Al $(H_2O)_6{}^{3+}$, respectively [42].

The SEM result of the extracted aluminum chloride hexahydrate crystals at 10 kV and 20 μm is shown in Figure 9(c). The morphology of crystals was irregular shape particles with some pseudohexagonal form and agglomerates of diverse sizes, which was also correlated with the literature [22]. In another study, the morphology of aluminum chloride hexahydrate crystals has been smooth surface and irregular particles shape [43].

3.5. Comparison of This Study with the Literature. Table 7 depicts the comparison of this study with the literature kinetics and activation energy of aluminum extraction from kaolinite using acid leaching. The kinetics of the extraction of aluminum from kaolinite of various origins showed different rate controlling step, kinetics model, and activation energy. The rate controlling steps and the kinetics model of the extraction of aluminum from Brazilian [8], Turkish [9], and Indonesian [44] kaolinites have been well fitted by shrinking core model of surface chemical reaction with first-order rate. On the other hand, kinetics model and the rate controlling steps of aluminum extraction from American [21] and Chinese [23] kaolinites have been well fitted by surface chemical reaction with nucleation growth model

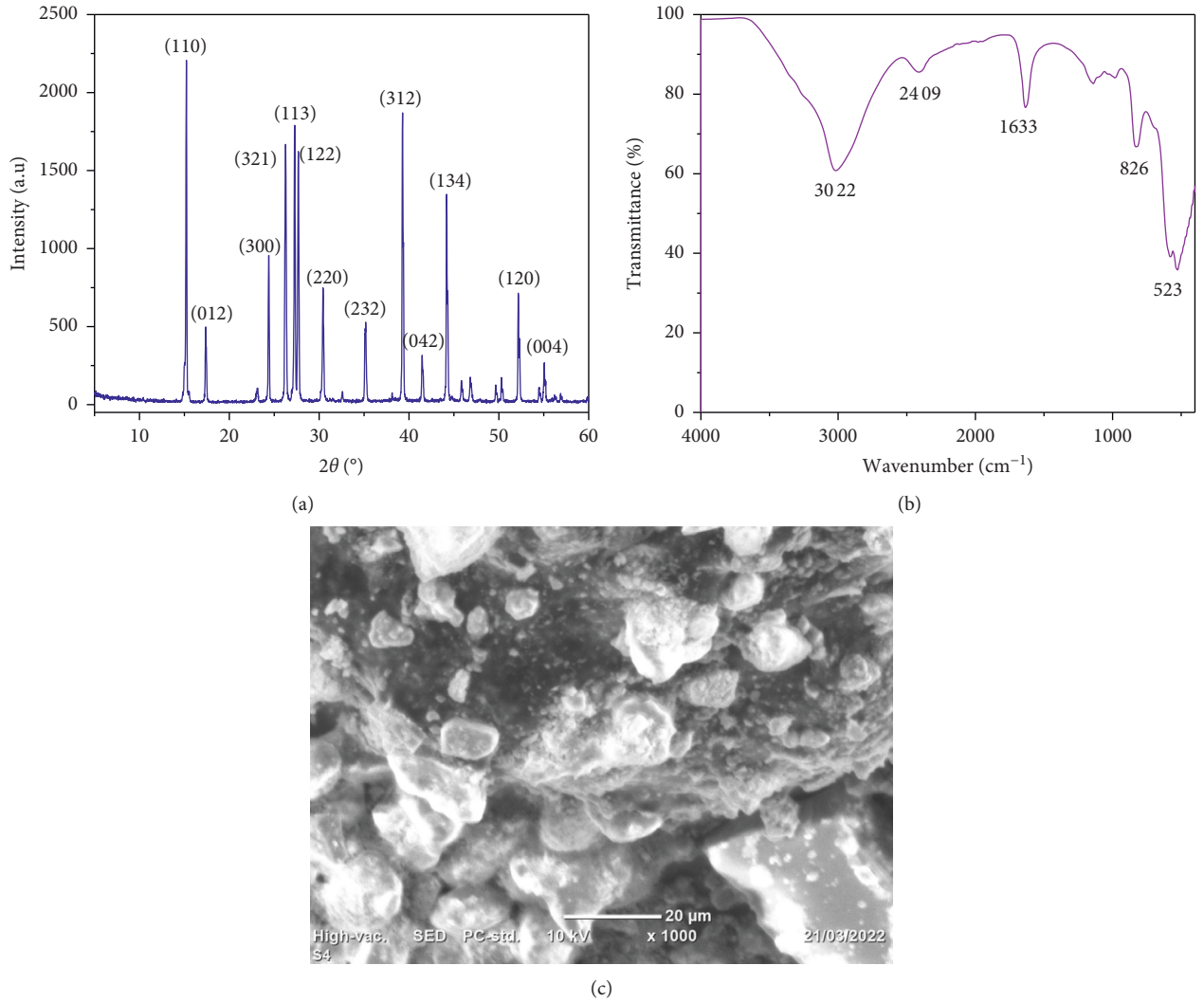

Figure 9: Extracted aluminum. (a) XRD peaks, (b) FTIR curve, and (c) SEM image of extracted aluminum chloride hexahydrate crystals extracted at 0.10 g·mL^{-1}, 5 M, 80°C, and 180 min.

Table 7: Comparison of this study with the literature kinetics and activation energy of aluminum extraction from kaolinite using acid leaching.

Origin of kaolinite	Extraction parameters	Maximum yield of Al (%)	Rate controlling step and kinetics model	Activation energy (kJ·mol^{-1})	References
Brazilian	0.88 M, 70–95°C, 10–180 min, and 0.05 g·mL^{-1}	98	Chemical reaction with first order and shrinking core model	90.6	[8]
Turkish	3–5 M, 45–96°C, 10–190 min, and 0.05 g·mL^{-1}	95.4	Chemical reaction with first order and shrinking core model	79.0	[9]
American	5.6 M, 60–95°C, 15–120 min, and 0.166 g·mL^{-1}	90	Chemical reaction and Avrami model	25.0	[21]
Chinese	1.6–8 M, 120–200°C, 10–100 min, and 0.067–0.2 g·mL^{-1}	98.7	Chemical reaction and Avrami model	16.3	[23]
Indonesian	4 M, 30–90°C, 10–60 min, and 0.02 g·mL^{-1}	91.3	Chemical reaction with first order and shrinking core model	19.2	[44]
Nigerian	0.5–3 M, 45–85°C, 20–100 min, and 0.062–0.250 g·mL^{-1}	70	Diffusion through liquid film and shrinking core model	35.3	[45]
Ethiopian	2–5 M, 50–80°C, 20–180 min, and 0.05–0.125 g·mL^{-1}	93%	Chemical reaction with first order and shrinking core model	25.4	This study

(Avrami model). In Nigerian kaolinite, the rate has been controlled by diffusion through liquid film [45]. The activation energies of aluminum extraction from Brazilian, Turkish, Indonesian, Nigerian, American, and Chinese kaolinites have been 90.6, 79.0, 35.3, 25.0, 19.2, and 16.3 $kJ \cdot mol^{-1}$, respectively. This study's kinetics model and rate controlling step were well fitted with shrinking core model of surface chemical reaction with first-order rate, which was in agreement with literature [8, 9, 44]. This study's activation energy (25.4 $kJ \cdot mol^{-1}$) was less than the activation energies of aluminum extractions from Brazilian, Turkish, and Nigerian kaolinites. However, this study's activation energy was higher than the activation energies of Indonesian and Chinese kaolinites. The reasons for the differences in the kinetics model, rate controlling step, and activation energy of aluminum extraction from various origins of kaolinites might be the variation of geographical location sources, calcination, and extraction process parameters.

4. Conclusion

The yield of aluminum extraction increased with increase of acid concentration, reaction temperature, and time and decreased as the solid-to-liquid ratio increased. The optimum aluminum extraction yield of 93% was obtained at the optimum extraction parameters of 5 M hydrochloric acid solution, 0.10 $g \cdot mL^{-1}$ solid-to-liquid ratio, and 80°C. The kinetics of aluminum extraction from kaolinite using hydrochloric acid were controlled by surface chemical reaction. The experimental results of this study were well fitted with the shrinking core model with first-order surface chemical reaction. The first-order reaction rate constants were 7.32×10^{-5}, 1.04×10^{-4}, 1.20×10^{-4}, and 1.70×10^{-4} $cm \cdot min^{-1}$ at 50, 60, 70, and 80°C, respectively. The apparent activation energy and the preexponential factor were 25.40 $kJ \cdot mol^{-1}$ and 0.949 $cm \cdot min^{-1}$, correspondingly. The crystallization efficiency and recovery of aluminum chloride hexahydrate crystals increased with volume of hydrochloric acid and crystallization time. The crystallization yield of aluminum chloride hexahydrate crystals reached 90%. This study clearly indicated that Ethiopian kaolinite could be a promising raw material to produce aluminum chloride hexahydrate, which could be used for water treatment application.

Data Availability

The datasets generated and/or analyzed during this study are available from the corresponding author upon reasonable request.

Conflicts of Interest

The authors declare that there are no conflicts of interest.

Authors' Contributions

All authors contributed to the study conception and design. Material preparation, data collection, and analysis were performed by Adamu Esubalew Kassa, Nurelegne Tefera Shibeshi, and Belachew Zegale Tizazu. The first draft of the manuscript was written by Adamu Esubalew Kassa and all authors commented on the draft versions of the manuscript. All authors read and approved the final manuscript.

Acknowledgments

The authors would like to thank Addis Ababa Science and Technology University for allowing experimental works and analytical instruments for characterization.

References

[1] D. Valeev, E. Mansurova, V. Bychinskii, and K. Chudnenko, "Extraction of alumina from high-silica bauxite by hydrochloric acid leaching using preliminary roasting method," *IOP Conference Series: Materials Science and Engineering*, vol. 110, pp. 1–6, 2016.

[2] D. V. Valeev, Y. A. Lainer, A. B. Mikhailova et al., "Reaction of bauxite with hydrochloric acid under autoclave conditions," *Metallurgist*, vol. 60, no. 1-2, pp. 204–211, 2016.

[3] D. Valeev, A. Shoppert, A. Mikhailova, and A. Kondratiev, "Acid and acid-alkali treatment methods of al-chloride solution obtained by the leaching of coal fly ash to produce sandy grade alumina," *Metals*, vol. 10, no. 5, pp. 585–618, 2020.

[4] Y. Guo, H. Lv, X. Yang, and F. Cheng, "$AlCl_3$ $6H_2O$ recovery from the acid leaching liquor of coal gangue by using concentrated hydrochloric inpouring," *Separation and Purification Technology*, vol. 151, pp. 177–183, 2015.

[5] D. Zinoveev, L. Pasechnik, M. Fedotov, V. Dyubanov, P. Grudinsky, and A. Alpatov, "Extraction of valuable elements from red mud with a focus on using liquid media-a review," *Recycling*, vol. 6, no. 2, pp. 38–32, 2021.

[6] L. Cui, F. Cheng, and J. Zhou, "Preparation of high purity $AlCl_3 \cdot 6H_2O$ crystals from coal mining waste based on iron (III) removal using undiluted ionic liquids," *Separation and Purification Technology*, vol. 167, pp. 45–54, 2016.

[7] Q. Yang, Q. Li, G. Zhang, Q. Shi, and H. Feng, "Investigation of leaching kinetics of aluminum extraction from secondary aluminum dross with use of hydrochloric acid," *Hydrometallurgy*, vol. 187, pp. 158–167, 2019.

[8] P. E. A. Lima, R. S. Angélica, and R. F. Neves, "Dissolution kinetics of amazonian metakaolin in hydrochloric acid," *Clay Minerals*, vol. 52, no. 1, pp. 75–82, 2017.

[9] M. R. Altiokka and H. L. Hoşgün, "Investigation of the dissolution kinetics of kaolin in HCl solution," *Hydrometallurgy*, vol. 68, no. 1-3, pp. 77–81, 2003.

[10] A. Ali, M. Al-Taie, and I. Ayoob, "The extraction of alumina from kaolin," *Engineering and Technology Journal*, vol. 37, no. 4A, pp. 133–139, 2019.

[11] S. Y. Gajam and S. Raghavan, "A kinetic model for the hydrochloric acid leaching of kaolinite clay in the presence of fluoride ions," *Hydrometallurgy*, vol. 15, no. 2, pp. 143–158, 1985.

[12] S. Aly, I. Ibrahim, and M. Abadir, "Utilization of kalapsha kaolin to prepare high purity alumina," *Egyptian Journal of Chemistry*, vol. 62, no. 9, pp. 1699–1712, 2019.

[13] E. G. Pinna, D. S. Suarez, G. D. Rosales, and M. H. Rodriguez, "Hydrometallurgical extraction of Al and Si from kaolinitic clays," *REM–International Engineering Journal*, vol. 70, no. 4, pp. 451–457, 2017.

[14] M. C. Gastuche, F. Toussaint, J. Fripiat, R. Touilleaux, and M. Van Meersche, "Study of intermediate stages in the kaolin⟶metakaolin transformation," *Clay Minerals*, vol. 5, no. 29, pp. 227–236, 1963.

[15] Y. Cheng, J. Xing, C. Bu et al., "Dehydroxylation and structural distortion of kaolinite as a high-temperature sorbent in the furnace," *Minerals*, vol. 9, no. 10, pp. 587–618, 2019.

[16] B. Ilic, A. Mitrovic, and L. Milicic, "Thermal treatment of kaolin clay to obtain metakaolin," *Chemical Industry*, vol. 64, no. 4, pp. 351–356, 2010.

[17] E. Erasmus, "The influence of thermal treatment on properties of kaolin," *Chemical Industry*, vol. 70, no. 5, pp. 595–601, 2016.

[18] U. Mark, C. N. Anyakwo, O. O. Onyemaobi, and C. S. Nwobodo, "Conditions for thermal activation of ngwo clay as an alternative resource for alumina," *Natural Resources*, vol. 10, no. 01, pp. 1–15, 2019.

[19] P. E. A. Lima, R. S. Angélica, and R. F. Neves, "Dissolution kinetics of amazonian metakaolin in nitric acid," *Cerâmica*, vol. 64, no. 369, pp. 86–90, 2018.

[20] P. E. A. Lima, R. S. Angélica, and R. F. Neves, "Dissolution kinetics of metakaolin in sulfuric acid: comparison between heterogeneous and homogeneous reaction methods," *Applied Clay Science*, vol. 88-89, pp. 159–162, 2014.

[21] S. F. Hulbert and D. E. Huff, "Kinetics of alumina removal from a calcined kaolin with nitric, sulphuric and hydrochloric acids," *Clay Minerals*, vol. 8, no. 3, pp. 337–345, 1970.

[22] V. I. Pak, S. S. Kirov, A. Y. Nalivaiko, D. Y. Ozherelkov, and A. A. Gromov, "Obtaining alumina from kaolin clay via aluminum chloride," *Materials*, vol. 12, no. 23, pp. 3938–4012, 2019.

[23] M. Lin, Y.-Y. Liu, S.-M. Lei, Z. Ye, Z.-Y. Pei, and B. Li, "High-efficiency extraction of Al from coal-series kaolinite and its kinetics by calcination and pressure acid leaching," *Applied Clay Science*, vol. 161, pp. 215–224, 2018.

[24] M. Yuan, X. Qiao, and J. Yu, "Phase equilibria of $AlCl_3 + FeCl_3 + H_2O$, $AlCl_3 + CaCl_2 + H_2O$, and $FeCl_3 + CaCl_2 + H_2O$ at 298.15 K," *Journal of Chemical and Engineering Data*, vol. 61, pp. 1749–1755, 2016.

[25] Y. Guo, X. Yang, H. Cui, F. Cheng, and F. Yang, "Crystallization behavior of $AlCl_3$ $6H_2O$ in hydrochloric system," *Huagong Xuebao/CIESC Journal*, vol. 65, pp. 3960–3967, 2014.

[26] M. Avrami, "Kinetics of phase change. *I* general theory," *The Journal of Chemical Physics*, vol. 7, no. 12, pp. 1103–1112, 1939.

[27] C. F. Dickinson and G. R. Heal, "Solid-liquid diffusion controlled rate equations," *Thermochimica Acta*, vol. 340-341, pp. 89–103, 1999.

[28] O. Levenspiel, *Chemical Reaction Engineering*, John Wiley & Sons, Hoboken, NJ, USA, 3rd edition, 1999.

[29] N. Demirkıran and A. Künkül, "Dissolution kinetics of ulexite in perchloric acid solutions," *International Journal of Mineral Processing*, vol. 83, no. 1-2, pp. 76–80, 2007.

[30] X. Ran, Z. Ren, H. Gao, R. Zheng, and J. Jin, "Kinetics of rare earth and aluminum leaching from kaolin," *Minerals*, vol. 7, no. 9, pp. 152–224, 2017.

[31] A. Mirwan, S. Susianto, A. Altway, and R. Handogo, "Kinetic model for identifying the rate controlling step of the aluminum leaching from peat clay," *Jurnal Teknologi*, vol. 80, no. 2, pp. 37–44, 2018.

[32] L. Ayele, J. Pérez-Pariente, Y. Chebude, and I. Díaz, "Synthesis of zeolite a from Ethiopian kaolin," *Microporous and Mesoporous Materials*, vol. 215, pp. 29–36, 2015.

[33] T. A. Aragaw and F. T. Angerasa, "Synthesis and characterization of Ethiopian kaolin for the removal of basic yellow (BY 28) dye from aqueous solution as a potential adsorbent," *Heliyon*, vol. 6, no. 9, Article ID e04975, 2020.

[34] T. M. Zewdie, I. Prihatiningtyas, A. Dutta, N. G. Habtu, and B. Van der Bruggen, "Characterization and beneficiation of Ethiopian kaolin for use in fabrication of ceramic membrane," *Materials Research Express*, vol. 8, no. 11, pp. 115201–115220, 2021.

[35] A. E. Kassa, N. T. Shibeshi, and B. Z. Tizazu, "Characterization and optimization of calcination process parameters for extraction of aluminum from Ethiopian kaolinite," *International Journal of Chemical Engineering*, vol. 2022, Article ID 5072635, 18 pages, 2022.

[36] E. J. Santos, E. B. Fantin, R. E. Paixão, A. B. Herrmann, and R. E. Sturgeon, "Spectrophotometric determination of aluminium in hemodialysis water," *Journal of the Brazilian Chemical Society*, vol. 26, pp. 2384–2388, 2015.

[37] W. Siriangkhawut, S. Tontrong, and P. Chantiratikul, "Quantitation of aluminium content in waters and soft drinks by spectrophotometry using eriochrome cyanine *R*," *Research Journal of Pharmaceutical, Biological and Chemical Sciences*, vol. 4, pp. 1155–1161, 2013.

[38] Y. Khanhuathon, W. Siriangkhawut, P. Chantiratikul, and K. Grudpan, "Spectrophotometric method for determination of aluminium content in water and beverage samples employing flow-batch sequential injection system," *Journal of Food Composition and Analysis*, vol. 41, pp. 45–53, 2015.

[39] O. Levenspiel, "Chemical reaction engineering," *Industrial and Engineering Chemistry Research*, vol. 38, no. 11, pp. 4140–4143, 1999.

[40] L. J. Wang and X. L. Xie, "Preparation and characterization of porous silica obtained by hydrochloric acid selective leaching metakaolinite," *Key Engineering Materials*, vol. 368-372, pp. 342–344, 2008.

[41] D. R. Buchanan and P. M. Harris, "A neutron and X-ray diffraction investigation of aluminum chloride hexahydrate," *Acta Crystallographica Section B Structural Crystallography and Crystal Chemistry*, vol. 24, no. 7, pp. 954–960, 1968.

[42] D. A. Riesgraf and M. L. May, "Infrared spectra of aluminum hydroxide chlorides," *Applied Spectroscopy*, vol. 32, no. 4, pp. 362–366, 1978.

[43] Y. Yang, N. Wang, X. Pang et al., "Thermodynamics of the decomposition of aluminum chloride hexahydrate to prepare alumina," *Journal of Materials Research and Technology*, vol. 15, pp. 6640–6646, 2021.

[44] A. Mirwan, S. Susianto, A. Altway, and R. Handogo, "Temperature-dependent kinetics of aluminum leaching from peat clay," *Malaysian Journal of Fundamental and Applied Sciences*, vol. 16, no. 2, pp. 248–251, 2020.

[45] H. O. Orugba, O. D. Onukwuli, A. K. Babayemi, and J. C. Umezuegbu, "Application of the shrinking core models to hydrochloric acid dissolution of alumina from clay," *ABUAD Journal of Engineering Research Development*, vol. 3, pp. 59–67, 2020.